# Thyroid Hormone T4 Mitigates Traumatic Brain Injury via Dynamically Remodeling Cell Type Specific Genes and Pathways

Guanglin Zhang[1], Graciel Diamante[1], In Sook Ahn[1], Zhe Ying[1], Nguyen Phi[1], Ning Wang[1], Douglas Arneson[1], Ingrid Cely[1], Kayla Arellano[1], Fernando Gomez Pinilla[1,3,4], Xia Yang[1,2,5,6,7]

[1]Department of Integrative Biology and Physiology, University of California, Los Angeles, Los Angeles CA 90095, USA.

[2]Bioinformatics Interdepartmental Program, University of California, Los Angeles, Los Angeles CA 90095, USA.

[3]Department of Neurosurgery, University of California, Los Angeles, Los Angeles CA 90095, USA.

[4]Brain Injury Research Center, University of California, Los Angeles, Los Angeles CA 90095, USA.

[5]Institute for Quantitative and Computational Biosciences, University of California, Los Angeles, Los Angeles CA 90095, USA.

[6]Molecular Biology Institute, University of California, Los Angeles, Los Angeles CA 90095, USA.

[7]Brain Research Institute, University of California, Los Angeles, Los Angeles CA 90095, USA.

Correspondence:

Xia Yang: xyang123@ucla.edu

Fernando Gomez-Pinilla: fgomezpi@ucla.edu

## Abstract

The complex pathology of traumatic brain injury (TBI) remains elusive due to the molecular and cellular dynamics that lead to cognitive impairments and neurological disorders. These complex attributes contribute to the difficulties in the success of TBI therapeutic regimens. Previously, we showed the spatiotemporal effects of TBI as well as the ability of T4 administration to prevent the cognitive impairments induced by TBI. Here, we focus on understanding the mechanism involved in the ability of T4 to prevent the cognitive damage induced by TBI using a systems level approach. Using single cell sequencing of two tissues (hippocampus and frontal cortex) at three stages post injury, we identified astrocytes, microglia, oligodendrocytes, and endothelial cells to be the most affected across both tissues and across timepoints after T4 treatment. We also identified key genes that were reversed after T4 treatment such as *Mbp* and *Plp1*. Oxidative phosphorylation, immune response, and nervous system related pathways were shown to be affected by T4 treatment. Our systems-level approach allows us to further understand the temporal and spatial dynamic reprogramming by T4 that prevents cognitive dysfunction induced by TBI.

## Introduction

Traumatic brain injury (TBI) caused by blunt hit such as bump, blow jolt to the head, or penetrating injury could lead to brain dysfunction. According to a CDC report, about 61,000 TBI-related deaths were recorded in 2019 which is around 166 deaths per day in the United States (https://wonder.cdc.gov/mcd.html.). Children who experience TBI generally have lower ability to participate in activities, poor mental health and learning performance [1-3]. Adults who have a TBI are at a higher risk for seizures [4], psychiatric disorders [5], and neurodegenerative diseases, such as Alzheimer's disease [6], Parkinson's disease [7]. Brain dysfunction due to TBI can persist for many years after injury adding a temporal aspect to disease pathology at acute, subacute, and chronic stages. In addition, previous studies in our lab showed TBI pathology to have a spatial component [8]. Different brain regions such as the hippocampus, which is important for learning and memory, and the frontal cortex, which is important for problem-solving, have been associated with TBI-induced brain dysfunction.

The factors contributing to the pathogenesis of TBI have been linked to excitotoxicity, mitochondrial dysfunction, oxidative stress, lipid peroxidation, neuroinflammation, axon degeneration, and apoptotic cell death [9]. Different regimens have been used to target TBI progression such as glutamate receptor antagonists, inhibitors of calcium-related signals, antioxidants, anti-inflammatory, and anti-apoptotic agents, and neurotrophic factors [10]. The different therapeutics that have been examined to treat the complications following TBI have had varying degrees of success.

Our previous studies using single-cell sequencing to investigate the cell-type specific dynamics of TBI revealed transthyretin (*Ttr*) as a potential therapeutic target [11]. *Ttr* encodes a transporter

for a thyroid hormone, thyroxine (T4). T4 is converted into the active hormone triiodothyronine (T3). Thyroid hormones have a role in many different physiological processes such as temperature regulation, energy balance and metabolism. Previously we showed that the administration of T4 significantly reversed the cognitive impairment caused by TBI [11], however, the exact mechanism has yet to be investigated.

Here, we focused on investigating the transcriptome and functional pathways following T4 intervention across different stages of TBI in different brain tissues at the single-cell level. We aim to understand the progression of TBI induced brain functional changes and the reversal of cognition loss by T4 administration.

## Materials and Methods

### Animals and fluid percussion injury (FPI) model

Male C57BL/6 J (B6) mice of 10 weeks old (Jackson Laboratory) weighing between 20 and 25 g were housed in cages (n = 4/group) and maintained under standard housing conditions (room temperature 22-24 °C) with 12 h light/dark cycle. Mice were randomly divided into either FPI or Sham group. The craniotomy was performed under a microscope (Leica), where a 3.0-mm diameter hole was made 2.5mm posterior to the bregma and 2.0mm lateral (left) of the midline with a high-speed drill (Dremel, Racine, WI, USA). The animal with intact dura was used for the following injury. A plastic cap was fixed over the hole with adhesive and dental cement. When the dental cement hardened, the cap was filled with 0.9% saline solution. Anesthesia was discontinued, and the injury cap was connected to the fluid percussion device. A fluid percussion

(1.5–1.7 atm, wake-up time greater than 5 min) was administered when the hind limb responded to a paw pinch. Sham animals underwent an identical preparation except for the percussion. The i.p. injection of T4 (1.2 ug/100g bodyweight) was administered at 1 hour and 6 hours post-FPI. Saline was injected as a control. Hippocampus and frontal cortex were dissected for use in Drop-seq (n = 3/group). The mice were sacrificed at indicated timepoints and the corresponding tissue was dissected for single-cell isolation. This study was performed following the National Institutes of Health Guide for the Care and Use of Laboratory Animals, USA. The experimental protocol was approved by the Chancellor's Animal Research Committee of the University of California at Los Angeles.

**Single-cell isolation**

Single-cell suspension was prepared according to the protocol by Brewer et al [12]. Briefly, the hippocampus and frontal cortex were dissected from the ipsilateral side of the brain, sliced into thin pieces, and transferred into 4 ml HABG medium containing Hibernate A, B27 supplement, and 0.5 mM Glutamax (Fisher Scientific, Hampton, NH, USA) and incubated in a water bath at 30 °C for 8 min. The tissue was incubated with prewarmed papain solution (2 mg/ml HA-Ca) at 30 °C for 30 min with shaking after removal of HABG medium. The papain solution was replaced with 2 ml prewarmed HABG. The tissue was triturated approximately ten times in 45s using a siliconized 9-in Pasteur pipette with a fire-polished tip. After 1min, the supernatant was gently transferred to the top of the prepared OptiPrep density gradient (Sigma Aldrich, St. Louis, MO, USA) without breaking the gradient. After centrifugation of 800 g for 15 min at 22 °C, the top 6 ml containing cellular debris was discarded. The bottom fraction was collected and

diluted with 5 ml HABG, 10 ml, especially for the cortex, and centrifuged for 3 min at 22 °C at 200 g followed by removal of the supernatant containing the debris. Finally, the cell pellet was loosened by flicking the tube and re-suspended in 1 ml 0.01% BSA (in PBS). The cell suspension was filtered through a 40-micron strainer (Fisher Scientific, Hampton, NH, USA) followed by cell counting.

**Single cell barcoding and library preparation**

Drop-seq was performed following the version 3.1 protocol from Macosko et al. [13]. We prepared the single-cell suspension at a final concentration of 100 cells/µl. The cell suspension, the oil (EvaGreen, Bio-Rad, Hercules, CA, USA), and the lysis buffer mixed with barcoded beads (ChemGenes, Wilmington, MA, USA) were co-flowed through a microfluidic device (FlowJEM, Toronto, Canada) at the fixed speeds (oil: 15,000 µl/h, cells: 4000 µl/h, and beads 4000 µl/h) to generate droplets. We dispensed 4000 beads into each PCR tube and ran 4+11 cycles. Pooled PCR tubes proceeded to cDNA library preparation. The cDNA library quality was checked using a BioAnalyzer high-sensitivity chip (Agilent, Santa Clara, CA, USA). The cDNA library was then fragmented and indexed using the Nextera DNA Library Preparation kit (Illumina, San Diego, CA, USA). The library quality mainly size and distribution were checked on a BioAnalyzer high-sensitivity chip and concentration was quantified by Qubit assays (ThermoFisher, Canoga Park, CA, USA) before sequencing.

**Sequencing of single cell library**

Sequencing was performed on an Illumina HiSeq 4000 (Illumina, San Diego, CA, USA) using the Drop-seq custom read 1B primer (GCC TGT CCG CGG AAG CAG TGG TAT CAA CGC AGA GTA C) (IDT, Coralville, IA, USA) and PE100 reads were generated. Read 1 consists of the 12 bp cell barcode, followed by the 8 bp UMI, and the last 80 bp on the read are not used. Read 2 contains the single-cell transcripts.

**Identification of cell clusters**

The Seurat V4 [14] was used for dimensional reduction and Louvain algorithm [15] was used for clustering the cells. The CCA [16] was performed to ensure that cell types were consistent across timepoints and treatments. The optimal cluster number was determined using Jackstraw permutation.

**Drop□seq data pre□processing and quality control**

The fastq files of the Drop-seq sequencing data were processed to digital expression gene matrices using Drop-seq tools version 1.13 (https:// github. com/ broad institute/ Drop-seq) and dropEst [8]. We followed the modified version of the snakemake-based dropSeqPipe (https://github.com/Hoohm/ dropSeqPipe) workflow as previously described [8]. Briefly, reads with low-quality barcodes were removed, and the cleaned reads were aligned to the mouse reference genome mm10 using STAR-2.5.0c. The reads which overlapped with exons were tagged using a RefFlat annotation file of mm10. To quantify the Chemgenes beads batch quality, we used the Drop-seq Tools function DetectBeadSynthesisErrors and estimated a bead synthesis

error rate of 5–10%, within the acceptable range. Finally, we generated a digital gene expression matrix for each sample where each row is the read count of a gene, and each column is a unique single cell. The transcript counts of each cell were normalized by the total number of UMIs for that cell. These values are then multiplied by 10,000 and log-transformed. Single cells were identified from background noise using a threshold of at least 200 genes and 300 transcripts.

**Identification of marker genes and cell identities of cell clusters**

Cell cluster-specific marker genes were identified using the FindConservedMarkers function in Seurat. Briefly, the Wilcoxon Rank Sum Test was performed within each set of samples and a meta p-value across all conditions was computed to assess the significance of each gene as a marker for a cluster. To be considered in the analysis, the gene had to be expressed in at least 10% of the single cells form one of the groups. Multiple testing was corrected using the Bonferroni method on the meta p-values. The genes with an adjusted p-value < 0.05 were defined as cell-type-specific marker genes.

**Identification of DEGs between sham control and TBI**

Differentially expressed genes (DEG) between sham control, TBI, and T4 samples within each identified cell type were analyzed using a Wilcoxon Rank Sum Test. For DEG analysis, we considered only the genes which were expressed in at least 10% of the cells from one of the two groups and there had to be at least a 0.25 log fold change in gene expression between the groups. DEGs were defined as genes with Bonferroni corrected adjusted p-value < 0.05 and these were

used in downstream pathway enrichment analysis. Enrichment of pathways from KEGG, Reactome, BIOCARTA, GO Molecular Functions, and GO Biological Processes was assessed with Fisher's exact test. Significant pathways were defined with the Benjamini–Hochberg corrected false discovery rate (FDR) < 0.05.

**Euclidean Distance**

First, we choose cells from control and treatment groups, and average every gene expression of each cell type from groups. The Euclidean distance was calculated using the average gene expression of each cell type between groups; Due to the high gene expression variation, we select the top 1000 genes and transform the gene expression using the Z-score for normalization. We generate a null distribution by sampling random cells of the given cell type from mixed groups 1000 times and compare the difference of Euclidean distance between the treatment effect and null distribution to determine the significance. The Bonferroni correction is used for multiple testing corrections across cell types.

## Results

### Identification of cell identities in two tissues across different post-TBI stages

To control the data quality, cells containing gene numbers between 200 and 3000, and that had mitochondrial content of less than 15% were used for analysis. This was done since an extremely high number of detected genes could indicate doublets and high proportions of mitochondrial content indicates damaged cells where cytoplasmic RNA is lost and the larger mitochondria are prone to stay inside [17].

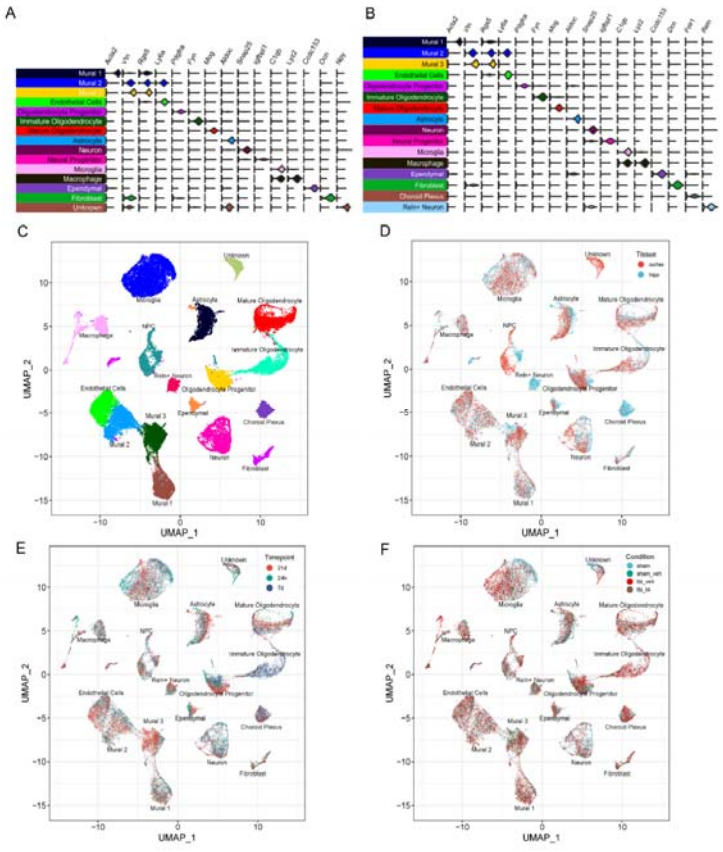


Figure 1. Cell identities and scRNAseq cell clusters. Expression of cell markers for each cell type in the frontal cortex (A) and hippocampus (B). UMAP embeddings of cells according to cell types (C), tissues (D; frontal cortex, hippocampus), timepoints (E; 24h, 7d, and 21d), and conditions (F; TBI vs sham, T4 vs TBI). Each point represents a single cell. Cells are clustered based

on transcriptome similarity using Louvain clustering, and cell types are identified using canonical markers and labeled on the plot. Within each tissue and timepoint, n = 3 animals per group.

After quality control, all cells were projected onto two dimensions using uniform manifold approximation and projection (UMAP). Cells with similar transcriptional expression patterns will be closer together forming a cluster. Canonical correlation analysis (CCA) was used to identify cell type marker genes consistent across different timepoints or conditions. Cell cluster identities were determined using canonical marker genes and Allen mouse brain atlas reference. Among these clusters, 14 cell types were identified in the hippocampus (Figure 1A) and 16 in the cortex (Figure 1B). These marker genes displayed distinct gene expression patterns across the cell types in the two brain regions. These 16 cell clusters (Figure 1C) showed similar gene expression distributions across tissues (Figure 1D) except choroid plexus and Rel+ neuron clusters which were unique to the hippocampus. We also observed a temporal transcriptional shift in microglia, astrocytes, mature oligodendrocytes, and oligodendrocyte progenitors across timepoints (Figure 1E). However, microglia showed a cluster shift across treatments (Figure 1F).

**The spatiotemporal shifts of the transcriptome in cell types following treatments across timepoints**

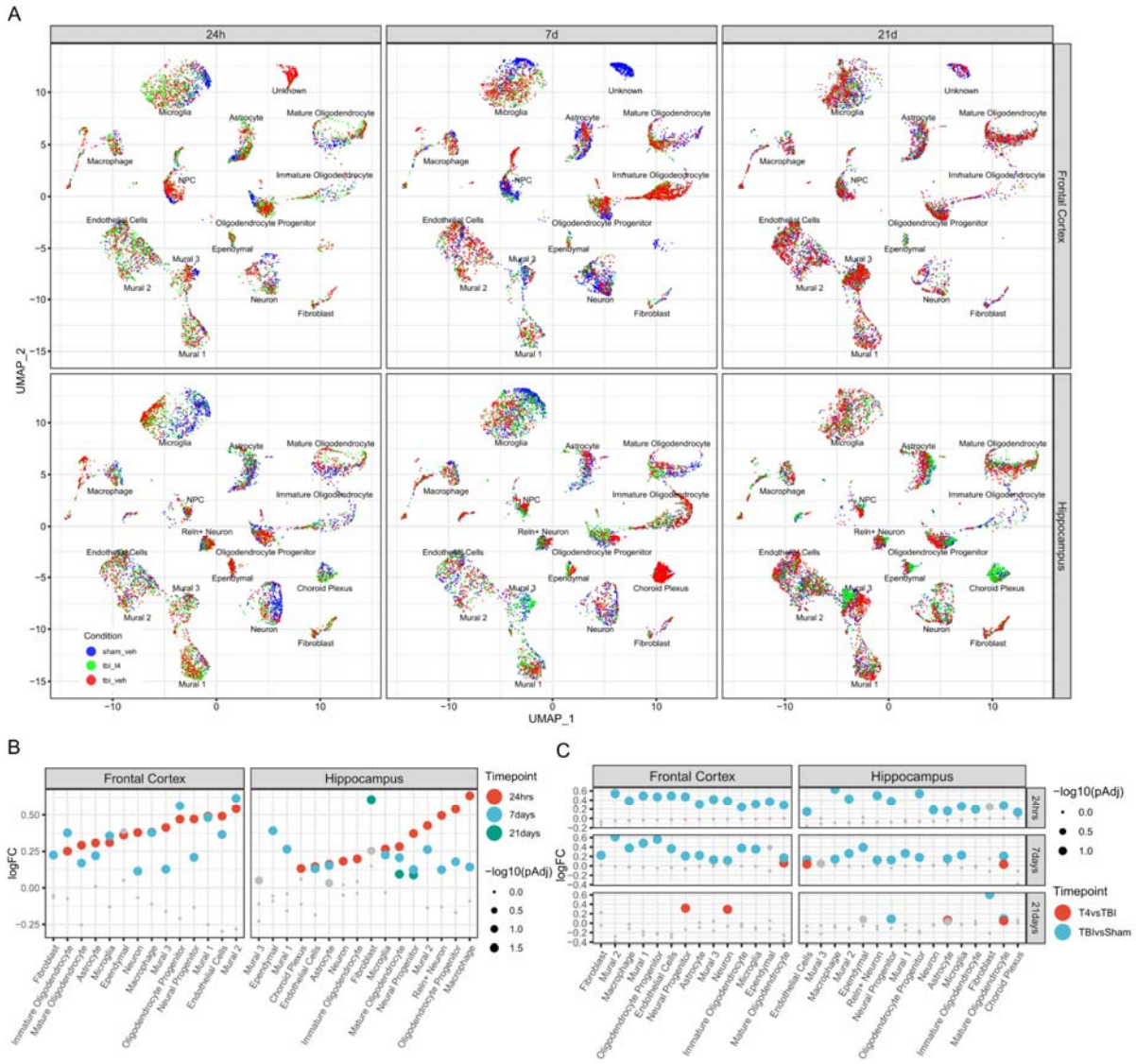


Figure 2. Transcriptomic shifts across cell types in the frontal cortex and hippocampus at 24 hours, 7 days, and 21days post-TBI and corresponding T4 treatment. UMAP embeddings (A) and Euclidean distance between TBI and sham (B) and between T4 and TBI (C) within cell types for each tissue and timepoints. The log fold change (logFC) quantifying the global transcriptome shift is labeled on the y-axis. Each point is colored by timepoint or treatment, and the size of each point relates to the adjusted p-value. Colored dots reach an adjusted p-value < 0.05 whereas gray points do not achieve statistical significance.

To qualify the transcriptomic shifts, we employed Euclidean distance which measures the distance in gene expression profiles of each cell type between treatment and control cells. The larger Euclidean distance is an indicator of stronger responses to treatment. Overall, we can see

that TBI caused transcriptomic shifts at the acute (21d) and subacute (7d) phases in the cortex across most of the cell types (Figure 2A, B). The distinct shift was also observed in the hippocampus across cell types at the acute phase, whereas the shift became milder at the subacute phase (Figure 2A, B). In contrast, we didn't see dramatic changes at the chronic (21d) phase across cell types in both the cortex and hippocampus, except for fibroblast, mature oligodendrocytes, and neural progenitor cells. As for T4 treatment, we observed a shift in mature oligodendrocytes of cortex and hippocampus and endothelial cells in the hippocampus at the subacute phase. Interestingly, neuron and neural progenitor cells of the cortex and astrocytes and mature oligodendrocytes in the hippocampus were the responsive cell types to T4 at the chronic phase.

**The spatiotemporal dynamics of DEGs**

To reveal the spatiotemporal responsiveness of cell types to TBI, we identified DEGs across cell type, tissues and timepoints (Figure 3). The extensive responses of these genes indicate that they might be involved in pathological processes of TBI. Based on DEG number, we found that astrocytes, microglia, and oligodendrocytes were consistently among the most affected cells in the hippocampus and cortex and across timepoints after TBI. The TBI effects on neurons in the hippocampus were highest at the early timepoint (24h) but decreased with time. However, in the cortex the highest DEG number for neurons was observed at 7d post TBI. After T4 treatment, astrocytes, microglia, oligodendrocytes and endothelial cells in general had the highest number of DEGs for both tissues and across timepoints. T4 treatment did different timepoint dynamics in the two tissues evaluated. For the hippocampus the highest number of DEGs were observed

largely in the 7d post-TBI (e.g. mature oligodendrocytes and oligodendrocyte progenitor cells) however, for cortex the number of DEGs increased with timepoint with 21d having the highest number of DEGs in certain cells (e.g. mature oligodendrocytes, endothelial cells and microglia).

Transthyretin (TTR), a serum transport protein, is responsible for T4 transfer to blood–brain barrier and plays a neuroprotective role in ischemia [18]. *Ttr* was upregulated at subacute phase across all the cell types of hippocampus which is consistent with previous finding that this gene was upregulated in most of cell types in the hippocampus in the early stage [8, 11]. Interestingly, it was downregulated across all cell types except choroid plexus at chronic phase. Some epidemiological studies have correlated low thyroid hormone levels with neurodegenerative diseases, where low thyroid hormone has negative effect on morbidity and mortality post CNS injury. The thyroid dysfunction in the elderly elevated the risk of developing neurodegenerative diseases and worse outcomes [19]. Population studies found the low serum free T3 is reversely related to the risk of Alzheimer's disease progression [20] and stroke severity, functional outcome and mortality [21].

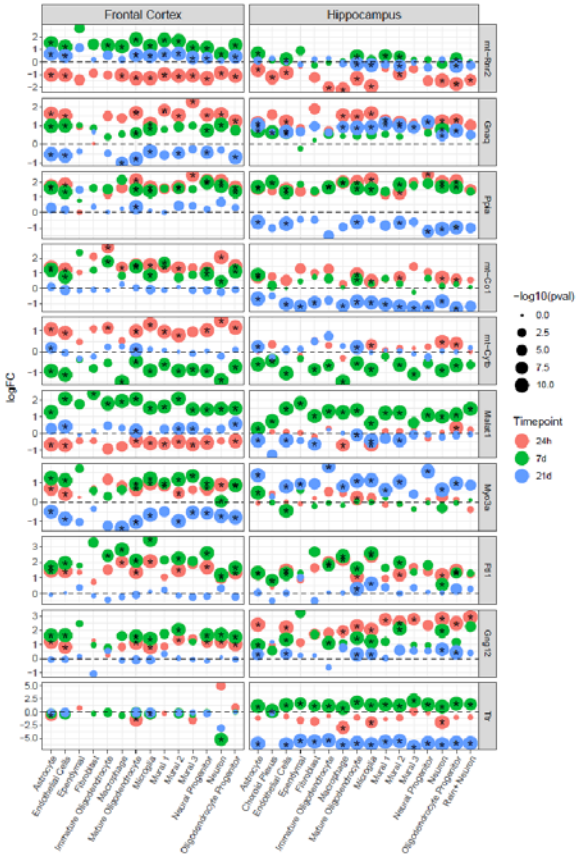


Figure 3. The top DEGs are significantly differentially expressed in most cell types across tissues and timepoints. Each row depicts a DEG. The genes which are significantly differentially expressed (adjusted p-value < 0.05) in specific cell types are indicated by a star. The color of each dot indicates the timepoint (24-h in red and 7-day in green, and 21-day in blue) at which the DEG was found, and the size of the dot corresponds to the −log10 (p-value). The y-axis is the log (fold change) of the gene between TBI and sham control cells within a particular cell type. Cell types are indicated on the x-axis.

In addition to *Ttr*, we also identified other top consistently expressed DEGs across cell types, such as *Ftl1*, *Gng12*, *Ppia*, and *Gnaq*. Ferritin light polypeptide 1 (*Ftl1*) and G protein subunit gamma 12 (*Gng12*) were significantly altered in majority of the identified cells of both the hippocampus and the cortex. *Ftl1* plays an important role in iron metabolism and storage and abnormal iron levels have been shown to be linked to neurodegenerative diseases [22]. *Gng12* encodes a protein that belongs to the Guanine nucleotide-binding protein (G proteins) family and has a role in pathways related to inflammation and cancer [23, 24]. Guanine nucleotide binding

protein, alpha q polypeptide (*Gnaq*) was consistently upregulated in many cells of the hippocampus while peptidylprolyl isomerase A (*Ppia*) was upregulated in the cells of the cortex. *Gnaq* is essential for transmembrane signaling and has been shown to be important for motor function and memory [25]. *Ppia* plays a role in protein folding and has been associated with nervous system degeneration [26].

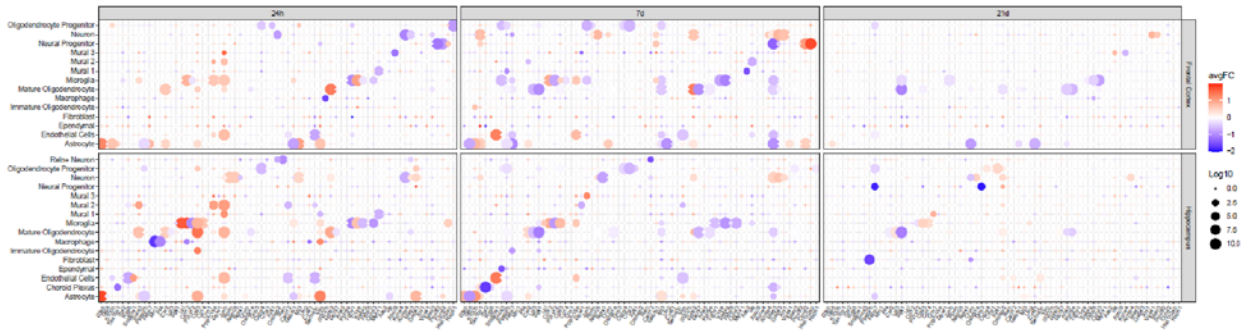

Figure 4. The top DEGs were significantly differentially expressed in a single cell type within a particular tissue and timepoint between TBI and sham. Each DEG is depicted in a separate column, and cell types are indicated by rows. The color of each dot indicates the log (fold change) of the bene between TBI and sham control cells (red indicates higher in TBI; cyan indicates lower in TBI) within a particular cell type. The size of each dot corresponds to the −log10(adjusted p-value).

The revelation of the cell type specific response is critical in understanding the cellular mechanisms associated with TBI-caused pathophysiology as well as exploration of cell-based therapeutic agents. The spatiotemporal dynamics of gene expression can track the progression of cellular response to TBI insult. Astrocytes are the most abundant cell type in the mammalian brain. Astrocyte activation or astrogliosis contributes to the response to various neurological insults and can pose a positive and negative effect on injury recovery, which indicates its regulation is tightly controlled [27]. *Gfap*, a marker for the activation of astrocytes, increased expression in both cortex and hippocampus at the acute phase and maintained upregulation only in the hippocampus at the subacute phase, which is consistent with our previous finding using

another dataset [11]. In contrast to the early stage, this gene returned to normal at the chronic phase in both the cortex and hippocampus. Astrocytes are coupled via gap junctions (GJs) comprising connexin 43 (*Gja1*) and connexin 30 (*Gjb6*), which facilitates intercellular ion exchange. Disruption of this coupling impairs the hippocampal synaptic plasticity and spatial learning and memory [28]. *Gjb6* was significantly reduced in both regions at the subacute phase. *Ccl12* was consistently upregulated in microglia across timepoints and two regions. This gene has been found increased in TBI mice brain and involved in modulation of complement pathway activator [29]. Other specific DEGs including *Tgfbr1*, *C1qa*, *Selplg*, and *P2ry12* which are microglia homeostatic signatures were also captured in the present study.

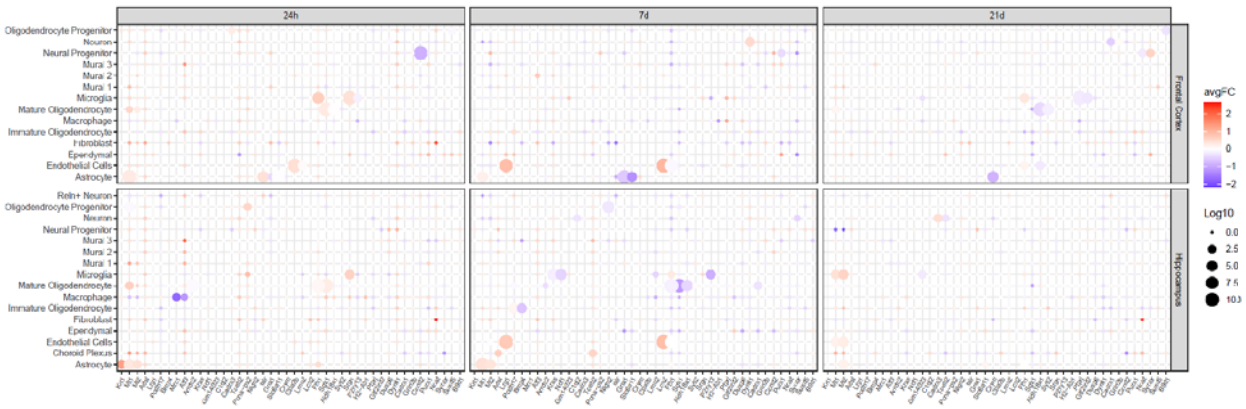


Figure 5. The top DEGs were significantly differentially expressed in a single cell type within a particular tissue and timepoint between T4 and TBI. Each DEG is depicted in a separate column, and cell types are indicated by rows. The color of each dot indicates the log (fold change) of the bene between TBI and sham control cells (red indicates higher in TBI; cyan indicates lower in TBI) within a particular cell type. The size of each dot corresponds to the −log10(adjusted p-value).

Metallothionein (MT) predominantly expressed in astrocytes especially in reactive astrocytes [30] has been implicated in processes related to neuroprotection, regeneration, and cognitive function [31, 32]. Loss of Mt1/2 has been associated with poor outcomes of several CNS injuries. We observed the significant increase of Mt1/Mt2 in astrocytes at acute and subacute

phases in both regions after T4 treatment. This upregulation was maintained in hippocampus until the chronic phase (Figure 5). *Lcn2* and *Lrg1* are top endothelial cell specific genes significantly induced at subacute phase. Increased LCN2 after ischemic stroke might maintain blood-brain barrier integrity through reducing damage to endothelial junctional proteins [33]. Primary and secondary injury caused by TBI may result in damage of the vasculature leading to subsequent cellular degeneration [34]. LRG1 is suggested to promote angiogenesis through upregulation of the TGF□β1 signaling pathway in ischemic rat brain [35]. LRG1 facilitated neovascularization through the transforming growth factor (TGF)-β1 signaling pathway in pathological blood vessel formation [36]. LRG1 may cause neurodegeneration in mouse cerebral cortex and may serve as a novel biomarker of neurodegenerative disease in human cerebrospinal fluid and [37].

**Functional annotation of DEGs**

To determine the functions these DEGs play in TBI pathogenesis and T4 intervention, we conducted pathway enrichment analysis using KEGG [38], Reactome[39], Biocarta, and Gene Ontology [40] databases to annotate these DEGs.

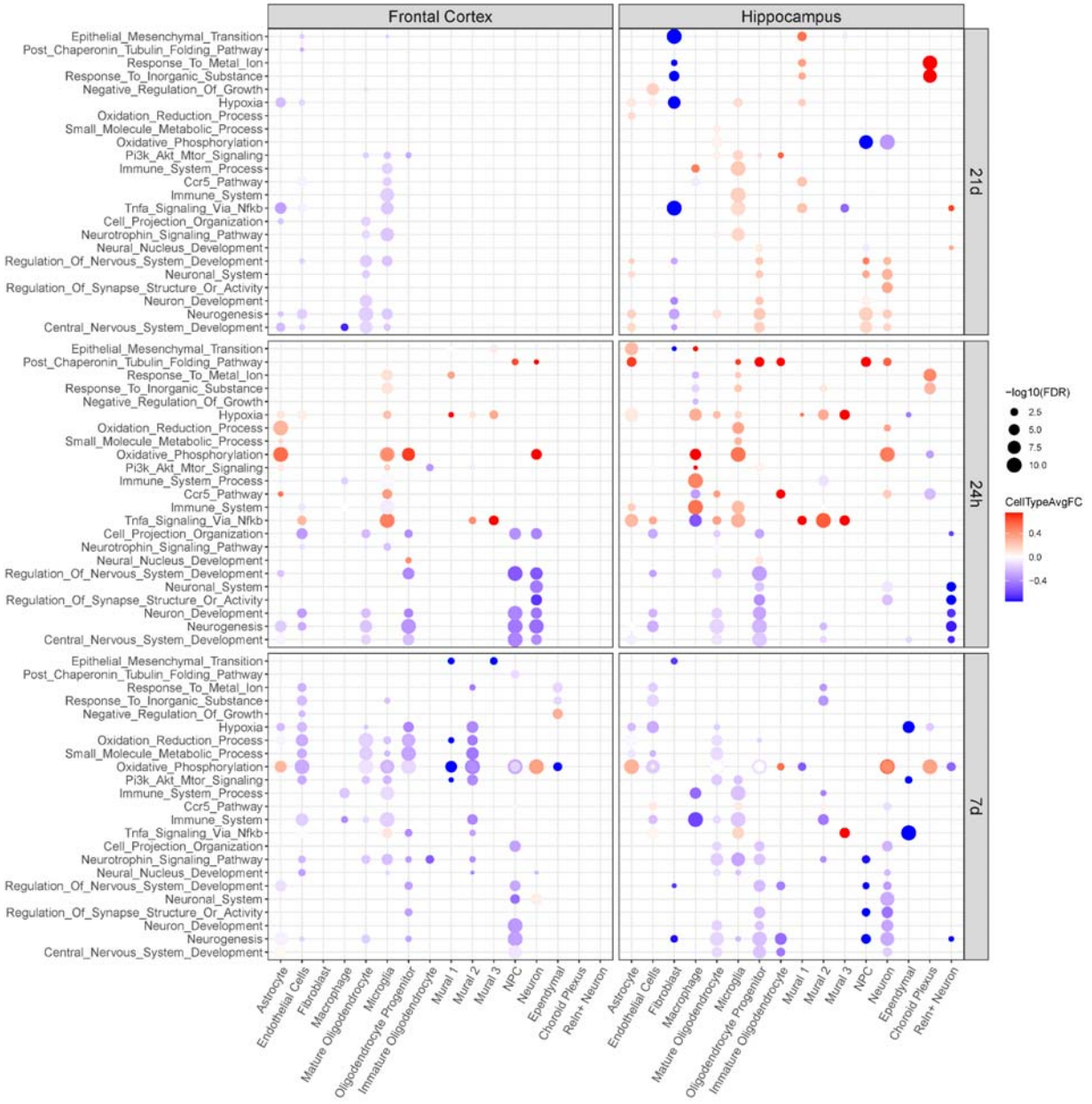


Figure 6. Top enriched pathways responsive to TBI across timepoint and tissues. Each dot is colored by the average log fold change between TBI vs sham control cells within that cell type for significant DEGs which overlap the indicated pathway. The size of each dot is proportional to the −log10(FDR). Cell types and pathways have been clustered with hierarchical clustering.

First, we explored the biological effects of TBI in the two tissues across the three different stages (Figure 6). Overall, pathway enrichment analysis displayed a dynamic pattern across timepoints. In the hippocampus, the acute and chronic phase post-TBI many pathways were upregulated

while the sub-acute phase showed mainly downregulated pathways. In the cortex, upregulated and downregulated pathways were more evenly distributed in the acute phase, while downregulated pathways were dominant in the subacute and chronic timepoints. Enrichment analysis showed pathways such as oxidative phosphorylation and TNFα signaling were among the affected pathways post TBI. Oxidative phosphorylation was consistently upregulated in astrocytes and neuron in both regions in both acute and subacute phases of TBI. In the chronic phase, it is downregulated in hippocampus and absent in cortex. In the astrocytes of the cortex, oxidative phosphorylation was highly upregulated at 24h, then milder effects were observed at 7d and then it was absent in 21d post TBI. In the astrocytes of the hippocampus, it was only significantly enriched at 7d.

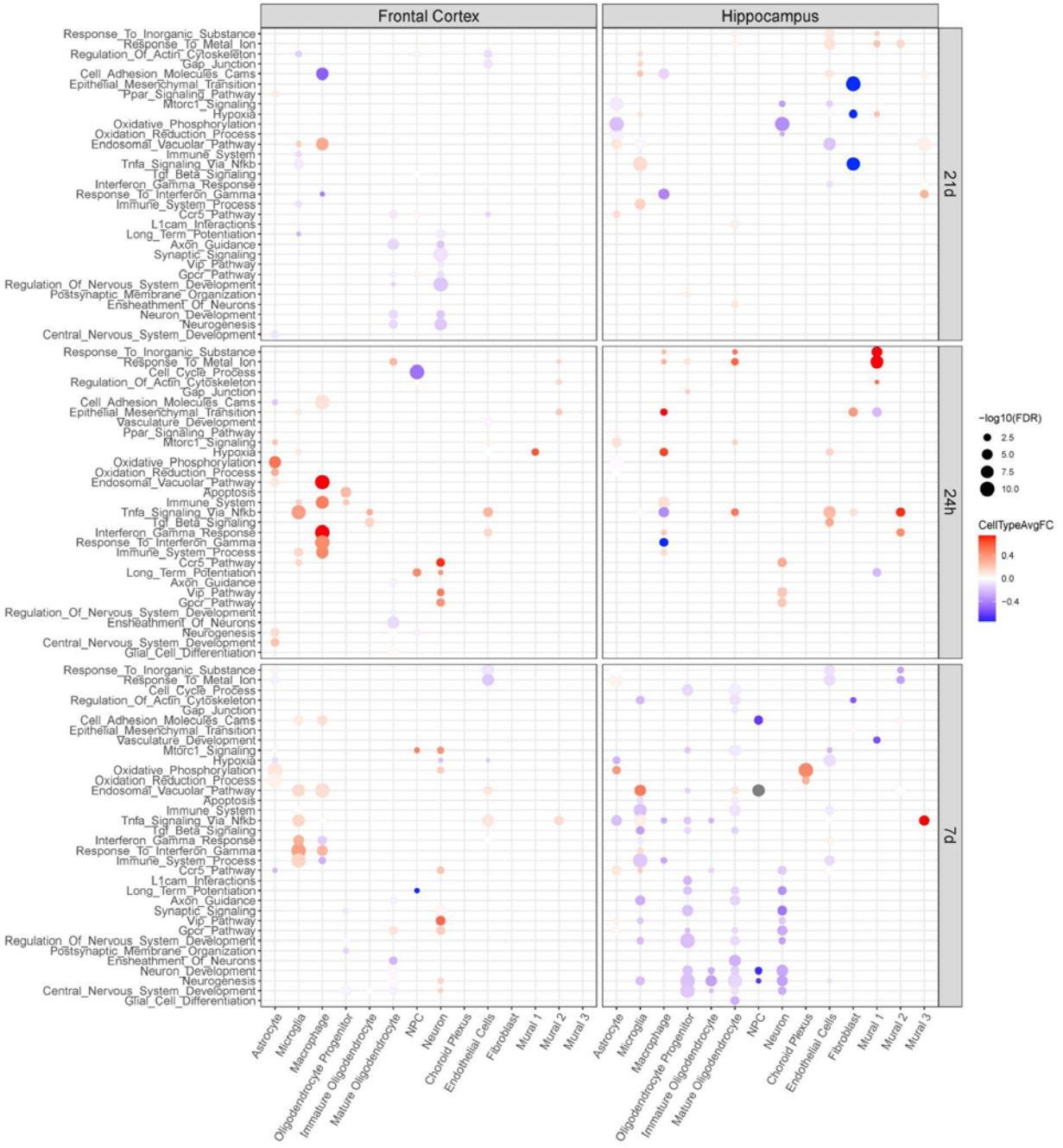


Figure 7. Top enriched pathways responsive to TBI across timepoint and tissues. Each dot is colored by the average log fold change between T4 vs TBI cells within that cell type for significant DEGs which overlap the indicated pathway. The size of each dot is proportional to the −log10(FDR). Cell types and pathways have been clustered with hierarchical clustering.

Next, we explored the enriched pathways potentially important for TBI brain dysfunction prevention by T4 (Figure 7). For example, oxidative phosphorylation was upregulated in

astrocytes of cortex during acute and subacute phases post-TBI and was further enhanced by T4 treatment. This was also observed in the hippocampus at the subacute phase. For immune related pathways such as TNFα via NFKB, CCR5 pathway, interferon Gamma response which were extensively elevated across immune cells of two regions 24h post-TBI, T4 treatment further elevated these pathways in the cortex, but not in the hippocampus. Interestingly, the immune response was suppressed in the cortex at subacute phase post-TBI but were enhanced after T4 treatment. In contrast, the immune response was suppressed in the hippocampus in TBI and was further downregulated by T4 treatment. Most genes of TNFα signaling via NFKB in microglia were upregulated 24h post-TBI, while T4 treatment reversed some of these genes, such as *Ler5*, *Jun*, *Junb*, *Marcks*, *Rhob*, and *Zfp36*, etc. We also found nervous system related pathways were inhibited in neural cell types of two regions during acute and subacute phases however, were reversed by T4 treatment in the acute and subacute phase in the cortex. Genes in neurogenesis of hippocampal neurons at subacute phase were downregulated post-TBI, which were mostly reversed by T4 treatment. Among these genes were *Mbp*, *Plp1*, *Cxcl12*, *Cdk5r1*, *Dpysl2*, *Gap43*, *Camk2b*, *Cpeb1*, *Gpm6a*, *Ncdn*, and *Nptx1*, many of which are involved in axon guidance and neuron projection. Hippocampal neurogenesis has been suggested to play a role in learning and memory [41]. Inhibiting neurogenesis after brain injury in mice [42] or after LFPI in rats [43] have been shown to impair spatial learning and cognitive recovery.

## Discussion

Our previous study, investigating the dynamics of TBI revealed transthyretin (*Ttr*) as a potential therapeutic target. *Ttr* encodes a protein that transports thyroxine (T4) throughout the body. Using a systems-level approach we investigated the specific effects of T4 treatment on TBI in two important brain regions (hippocampus and frontal cortex) and three post injury stages (acute, subacute, and chronic). Our study provides insights into the spatiotemporal gene regulation after TBI that potentially drives disease progression and sheds light on the important cells and pathways that are involved in the ability of thyroid hormone T4 to reverse TBI effects. Our data showed astrocytes, microglia, oligodendrocytes and endothelial cells to be important for T4 dependent reversion, which was among the sensitive cells post TBI. Enrichment analysis showed pathways such as oxidative phosphorylation, immune response and nervous system related pathways to be affected by T4 treatment. Our results provide further insights on potential therapeutics to prevent progression of TBI-induced brain dysfunction.

Previously, we showed the ability of T4 administration to prevent the cognitive impairments induced by TBI. Using the Barnes Maze test mice treated with T4 did not have learning and memory problems 7 days post TBI. Interestingly, when we compare the transcriptome of T4 treated mice with the TBI group, we found the 7d time point to have the biggest number in DEGs in the hippocampus. In addition, *Ttr* gene expression alterations are consistently observed in the hippocampus compared to the frontal cortex both in our current data and previous results. Our data suggest that mature oligodendrocytes and oligodendrocyte progenitor cells in the hippocampus to play an important role in T4 reversion. Oligodendrocytes play a role in myelin assembly in CNS by wrapping around neuron axons which ensures the fast conduction of nerve impulse [44] and metabolic support [45, 46]. TBI could cause the progressive demyelination and

degeneration of axons within white matter tracts [47]. The remyelination is fulfilled mainly by newly generated oligodendrocytes [48]. Oligodendrocyte progenitors contribute to remyelination and glial scar formation. The contribution of mature oligodendrocytes to remyelination is under debate as they are differentiated and immobile [49, 50]. However, recent findings suggest that intact, mature oligodendrocytes are involved in remyelination following injury [51, 52]. Myelin plasticity may be the underlying mechanism of TBI pathogenesis and one of T4 targets.

We observed that induced oxidative phosphorylation in astrocytes of cortex was further enhanced by thyroid hormone treatment during acute and subacute phases. Thyroid hormone is well known as the endocrine controller of normal growth and development as well as metabolism through metabolic and respiratory rates on almost all nucleated cells in mammals [53]. In term of metabolic regulation, we found astrocyte was the main responsive cell type to T4 which implies the priority of T4 target in this setting. Astrocytes morphologically bridge neuron and blood vessel to fine tune the coordination between neuronal activity and metabolic supply [54]. Astrocytes have suggested to be responsible for 5%-15% of ATP consumption of the brain [55]. Instead of production of ATP via oxidative phosphorylation [56], astrocyte mainly depends on glycolysis to produce lactate, which is considered as important energy source for neuronal mitochondrial respiration [57]. Although astrocytes with oxidative phosphorylation defects didn't affect long-term survival, but lead to neurodegeneration after ischemia due to failure to reactive astrocyte proliferation which is vital for supporting neurons [58]. In our findings the T4 enhanced oxidative phosphorylation may indicate that T4 protected the neurons from the damage caused by TBI through promoting the proliferation of reactive astrocytes.

In summary, our investigation across tissues and timepoints offers a comprehensive understanding of the cellular and molecular pathways in T4 induced reversal of TBI dysfunction

using advanced single cell technologies. Our data not only advances our knowledge in using T4 as part of TBI regimen but also gives a broader understanding on other TBI therapies. We identified important cell types and pathways in TBI and T4 treatment that can be used to help prioritize therapies to mitigate TBI associated neurological effects. We do acknowledge that future studies need to be done to understand their causal role in protecting from TBI induced effects.

**Funding** X.Y. and F.G-P. are funded by R01 NS117148. F.G-P. is funded by R01 NS50465.

**Declarations**

Conflict of interest: The authors declare no conflict of interest.

Consent for publication: All authors have given their consent for publication.

## References


1. Bedell, G.M. and H.M. Dumas, *Social participation of children and youth with acquired brain injuries discharged from inpatient rehabilitation: a follow-up study.* Brain Inj, 2004. **18**(1): p. 65-82.
2. Rivara, F.P., et al., *Incidence of disability among children 12 months after traumatic brain injury.* Am J Public Health, 2012. **102**(11): p. 2074-9.
3. Rivara, F.P., et al., *Persistence of disability 24 to 36 months after pediatric traumatic brain injury: a cohort study.* J Neurotrauma, 2012. **29**(15): p. 2499-504.
4. Annegers, J.F., et al., *A population-based study of seizures after traumatic brain injuries.* N Engl J Med, 1998. **338**(1): p. 20-4.
5. Ponsford, J., Y. Alway, and K.R. Gould, *Epidemiology and Natural History of Psychiatric Disorders After TBI.* J Neuropsychiatry Clin Neurosci, 2018. **30**(4): p. 262-270.
6. Lye, T.C. and E.A. Shores, *Traumatic brain injury as a risk factor for Alzheimer's disease: a review.* Neuropsychol Rev, 2000. **10**(2): p. 115-29.
7. Goldman, S.M., et al., *Head injury and Parkinson's disease risk in twins.* Ann Neurol, 2006. **60**(1): p. 65-72.
8. Arneson, D., et al., *Systems spatiotemporal dynamics of traumatic brain injury at single-cell resolution reveals humanin as a therapeutic target.* Cell Mol Life Sci, 2022. **79**(9): p. 480.
9. Ray, S.K., C.E. Dixon, and N.L. Banik, *Molecular mechanisms in the pathogenesis of traumatic brain injury.* Histol Histopathol, 2002. **17**(4): p. 1137-52.
10. Ng, S.Y. and A.Y.W. Lee, *Traumatic Brain Injuries: Pathophysiology and Potential Therapeutic Targets.* Front Cell Neurosci, 2019. **13**: p. 528.
11. Arneson, D., et al., *Single cell molecular alterations reveal target cells and pathways of concussive brain injury.* Nat Commun, 2018. **9**(1): p. 3894.
12. Brewer, G.J. and J.R. Torricelli, *Isolation and culture of adult neurons and neurospheres.* Nat Protoc, 2007. **2**(6): p. 1490-8.
13. Macosko, E.Z., et al., *Highly Parallel Genome-wide Expression Profiling of Individual Cells Using Nanoliter Droplets.* Cell, 2015. **161**(5): p. 1202-1214.
14. Hao, Y., et al., *Integrated analysis of multimodal single-cell data.* Cell, 2021. **184**(13): p. 3573-3587 e29.
15. Blondel, V.D., et al., *Fast unfolding of communities in large networks.* Journal of Statistical Mechanics-Theory and Experiment, 2008.
16. Han, X., et al., *Mapping the Mouse Cell Atlas by Microwell-Seq.* Cell, 2018. **172**(5): p. 1091-1107 e17.
17. Lun, A.T., D.J. McCarthy, and J.C. Marioni, *A step-by-step workflow for low-level analysis of single-cell RNA-seq data with Bioconductor.* F1000Res, 2016. **5**: p. 2122.
18. Santos, S.D., et al., *CSF transthyretin neuroprotection in a mouse model of brain ischemia.* J Neurochem, 2010. **115**(6): p. 1434-44.
19. Biondi, B., A.R. Cappola, and D.S. Cooper, *Subclinical Hypothyroidism: A Review.* JAMA, 2019. **322**(2): p. 153-160.
20. Quinlan, P., et al., *Low serum concentration of free triiodothyronine (FT3) is associated with increased risk of Alzheimer's disease.* Psychoneuroendocrinology, 2019. **99**: p. 112-119.
21. Lamba, N., et al., *A prognostic role for Low tri-iodothyronine syndrome in acute stroke patients: A systematic review and meta-analysis.* Clin Neurol Neurosurg, 2018. **169**: p. 55-63.
22. Muhoberac, B.B. and R. Vidal, *Abnormal iron homeostasis and neurodegeneration.* Front Aging Neurosci, 2013. **5**: p. 32.
23. Larson, K.C., et al., *Gng12 is a novel negative regulator of LPS-induced inflammation in the microglial cell line BV-2.* Inflamm Res, 2010. **59**(1): p. 15-22.

24. Liu, R., et al., *GNG12 as A Novel Molecular Marker for the Diagnosis and Treatment of Glioma.* Front Oncol, 2022. **12**: p. 726556.
25. Frederick, A.L., T.P. Saborido, and G.D. Stanwood, *Neurobehavioral phenotyping of G(alphaq) knockout mice reveals impairments in motor functions and spatial working memory without changes in anxiety or behavioral despair.* Front Behav Neurosci, 2012. **6**: p. 29.
26. Lauranzano, E., et al., *Peptidylprolyl isomerase A governs TARDBP function and assembly in heterogeneous nuclear ribonucleoprotein complexes.* Brain, 2015. **138**(Pt 4): p. 974-91.
27. Pekny, M. and M. Pekna, *Astrocyte reactivity and reactive astrogliosis: costs and benefits.* Physiol Rev, 2014. **94**(4): p. 1077-98.
28. Hosli, L., et al., *Decoupling astrocytes in adult mice impairs synaptic plasticity and spatial learning.* Cell Rep, 2022. **38**(10): p. 110484.
29. Popiolek-Barczyk, K., et al., *The CCL2/CCL7/CCL12/CCR2 pathway is substantially and persistently upregulated in mice after traumatic brain injury, and CCL2 modulates the complement system in microglia.* Mol Cell Probes, 2020. **54**: p. 101671.
30. Holloway, A.F., et al., *Localisation and expression of metallothionein immunoreactivity in the developing sheep brain.* Int J Dev Neurosci, 1997. **15**(2): p. 195-203.
31. West, A.K., et al., *Metallothionein in the central nervous system: Roles in protection, regeneration and cognition.* Neurotoxicology, 2008. **29**(3): p. 489-503.
32. Giralt, M., et al., *Metallothionein-1+2 deficiency increases brain pathology in transgenic mice with astrocyte-targeted expression of interleukin 6.* Neurobiol Dis, 2002. **9**(3): p. 319-38.
33. Du, Y., et al., *Effects of lipocalin-2 on brain endothelial adhesion and permeability.* PLoS One, 2019. **14**(7): p. e0218965.
34. Jullienne, A., et al., *Chronic cerebrovascular dysfunction after traumatic brain injury.* J Neurosci Res, 2016. **94**(7): p. 609-22.
35. Meng, H., et al., *LRG1 promotes angiogenesis through upregulating the TGFbeta1 pathway in ischemic rat brain.* Mol Med Rep, 2016. **14**(6): p. 5535-5543.
36. Wang, X., et al., *LRG1 promotes angiogenesis by modulating endothelial TGF-beta signalling.* Nature, 2013. **499**(7458): p. 306-11.
37. Miyajima, M., et al., *Leucine-rich alpha2-glycoprotein is a novel biomarker of neurodegenerative disease in human cerebrospinal fluid and causes neurodegeneration in mouse cerebral cortex.* PLoS One, 2013. **8**(9): p. e74453.
38. Kanehisa, M. and S. Goto, *KEGG: kyoto encyclopedia of genes and genomes.* Nucleic Acids Res, 2000. **28**(1): p. 27-30.
39. Croft, D., et al., *The Reactome pathway knowledgebase.* Nucleic Acids Res, 2014. **42**(Database issue): p. D472-7.
40. Gene Ontology, C., *Gene Ontology Consortium: going forward.* Nucleic Acids Res, 2015. **43**(Database issue): p. D1049-56.
41. Jessberger, S., et al., *Dentate gyrus-specific knockdown of adult neurogenesis impairs spatial and object recognition memory in adult rats.* Learn Mem, 2009. **16**(2): p. 147-54.
42. Blaiss, C.A., et al., *Temporally specified genetic ablation of neurogenesis impairs cognitive recovery after traumatic brain injury.* J Neurosci, 2011. **31**(13): p. 4906-16.
43. Sun, D., et al., *Inhibition of injury-induced cell proliferation in the dentate gyrus of the hippocampus impairs spontaneous cognitive recovery after traumatic brain injury.* J Neurotrauma, 2015. **32**(7): p. 495-505.
44. Nave, K.A. and H.B. Werner, *Myelination of the nervous system: mechanisms and functions.* Annu Rev Cell Dev Biol, 2014. **30**: p. 503-33.
45. Lee, Y., et al., *Oligodendroglia metabolically support axons and contribute to neurodegeneration.* Nature, 2012. **487**(7408): p. 443-8.
46. Saab, A.S., et al., *Oligodendroglial NMDA Receptors Regulate Glucose Import and Axonal Energy Metabolism.* Neuron, 2016. **91**(1): p. 119-32.

47. Mierzwa, A.J., et al., *Components of myelin damage and repair in the progression of white matter pathology after mild traumatic brain injury.* J Neuropathol Exp Neurol, 2015. **74**(3): p. 218-32.
48. Franklin, R.J.M. and C. Ffrench-Constant, *Regenerating CNS myelin - from mechanisms to experimental medicines.* Nat Rev Neurosci, 2017. **18**(12): p. 753-769.
49. Crawford, A.H., et al., *Pre-Existing Mature Oligodendrocytes Do Not Contribute to Remyelination following Toxin-Induced Spinal Cord Demyelination.* Am J Pathol, 2016. **186**(3): p. 511-6.
50. Pukos, N., et al., *Myelin status and oligodendrocyte lineage cells over time after spinal cord injury: What do we know and what still needs to be unwrapped?* Glia, 2019. **67**(11): p. 2178-2202.
51. Duncan, I.D., et al., *The adult oligodendrocyte can participate in remyelination.* Proc Natl Acad Sci U S A, 2018. **115**(50): p. E11807-E11816.
52. Macchi, M., et al., *Mature oligodendrocytes bordering lesions limit demyelination and favor myelin repair via heparan sulfate production.* Elife, 2020. **9**.
53. Brent, G.A., *Mechanisms of thyroid hormone action.* J Clin Invest, 2012. **122**(9): p. 3035-43.
54. Zhao, Z., et al., *Establishment and Dysfunction of the Blood-Brain Barrier.* Cell, 2015. **163**(5): p. 1064-1078.
55. Belanger, M., I. Allaman, and P.J. Magistretti, *Brain energy metabolism: focus on astrocyte-neuron metabolic cooperation.* Cell Metab, 2011. **14**(6): p. 724-38.
56. McAvoy, K. and H. Kawamata, *Glial mitochondrial function and dysfunction in health and neurodegeneration.* Mol Cell Neurosci, 2019. **101**: p. 103417.
57. Bolanos, J.P., *Bioenergetics and redox adaptations of astrocytes to neuronal activity.* J Neurochem, 2016. **139 Suppl 2**: p. 115-125.
58. Fiebig, C., et al., *Mitochondrial Dysfunction in Astrocytes Impairs the Generation of Reactive Astrocytes and Enhances Neuronal Cell Death in the Cortex Upon Photothrombotic Lesion.* Front Mol Neurosci, 2019. **12**: p. 40.